Supporting Information

Dong et al. 10.1073/pnas.1718910115

SI Materials and Methods

Determination of K_M^{NADH} and Rates of Heat Denaturation. Enzyme preparation involved ammonium sulfate precipitation of heat-treated homogenates (heating removed the thermally labile mitochondrial paralog; mMDH) to isolate a cMDH-rich protein fraction (1). Dialyzed aliquots of the ammonium sulfate precipitated proteins were used for assays. We chose to focus on binding of the cofactor (NADH), rather than substrate (malate or oxaloacetate) because of the wealth of data available for comparative analyses of cofactor binding (1–3). The catalytic rate constant (k_{cat}) was not determined because we used only a partially purified cMDH. Binding of NADH to cMDH was indexed by the apparent Michaelis–Menten constant, K_M^{NADH}. The reaction mixture contained imidazole–Cl buffer (200 mmol/L with a pH value of 7.0 at 20 °C), oxaloacetic acid (200 μmol/L), and different concentrations of NADH (10, 15, 20, 30, 40, 60, and 75 μmol/L) (1). K_M^{NADH} values were calculated from the initial velocities of the reaction at each NADH concentration by using Prism software (Version 5.0; GraphPad Software). Thermal stabilities were carried out as described by Fields et al. (3). Dialyzed enzyme preparations were heated at 42.5 °C for different periods of time. Aliquots were removed and assayed for residual cMDH activity.

Sequencing of cMDH cDNA. To obtain the data needed for the MDS analyses, we sequenced all of the cMDH orthologs that had not previously been sequenced. The protocols used for sequencing the cDNAs followed those of Fields et al. (3), Dong and Somero (1), and Liao et al. (4). Total RNA was purified from foot muscle by using TRIzol reagent (Invitrogen). Reverse-transcriptase (RT) reactions were performed by using PrimeScript RT reagent kits (TaKaRa). The PCR was used to amplify the partial sequences of cDNA of cMDH by using pairs of primers (Table S4). The full-length cDNAs were obtained by using the 5′ and 3′ rapid amplification of cDNA ends (RACE) protocol (Clontech Laboratories, Inc.). Pairs of 5′ and 3′ gene-specific primers (Table S4) were designed based on the partial sequences above. The PCR was used to amplify the 5′ and 3′ ends of the cDNAs. RACE PCR products were amplified with the SeqAmp DNA polymerase and cloned into the linearized pRACE vector with the In-Fusion HD Cloning and Stellar Competent Cells kit (Clontech Laboratories, Inc.). Based on the 5′ and 3′ untranslated regions, pairs of primers (Table S4) were designed to amplify the full-length cDNA coding regions. The full-length cDNA sequences were amplified and sequenced (Invitrogen Biotechnology Co.). The cDNA sequences were assembled by using DNAMAN software (Lynnon Biosoft), and the deduced amino acid sequences were aligned by using the ClustalX2 algorithm (5). The GenBank accession numbers are shown in Table S5.

Molecular Modeling of cMDH cDNA. By using the sequence data, 3D models were constructed by the I-TASSER server with a high C-score level (~1.6). C-score is a confidence score for estimating the quality of predicted models by I-TASSER, which is typically in the range between −5 and 2, and a higher value signifies a model with a high confidence (6).

MDS of cMDH. The computed 3D structures constructed above were used as the starting models of the simulations. Simulations were performed by using NAMD (Version 2.9) (7) with the CHARMM36 force field (7–10). Transferable intermolecular potential 3P water was used as the aqueous solution to create simulation conditions that more closely resembled the cellular environment (11). The proteins were first placed into separate suitably sized simulation cubic boxes and solvated with simple point-charged water molecules. The size of the water box was created with a layer of water 10 Å in each direction from the atom with the largest coordinate in that direction. Na^+ and Cl^- ions were used as the counterions to neutralize the negative charges of proteins. The solvated systems were subjected to energy minimization to remove energetically unfavorable contacts among water molecules and ions (steepest descent method, 5,000 steps). Each system was performed in the isobaric-isothermal (NPT) ensemble at 1 bar pressure and the set temperature by the Langevin Piston and Langevin Dynamic method, respectively. The SHAKE algorithm was used to constrain bond length with a time step of 2 fs (12). Long-range interaction was applied by using the particle mesh Ewald method (13). Local interaction distance common to both electrostatic and van der Waals calculations (cutoff) was 12 Å. For all simulations, each system was assigned for 20 ns at 15 and 42 °C in triplicate. Trajectories of the structures were collected every 0.002 ns. Every 0.002 ns of the actual frame was stored during the simulation.

The VMD program was used to visualize and analyze the simulation trajectories (14). The rmsd of backbone atom positions and the RMSF for individual residues in all models were calculated and compared. For rmsd and RMSF calculations, the initial and energy-minimized structures, respectively, were used as the reference. They are defined as: $\mathrm{RMSD} = \sqrt{1/N\sum_{i=1}^{N}(r_i - r_0)^2}$ and $\mathrm{RMSF} = \sqrt{1/N\sum_{i=1}^{N}(r_i - r)^2}$, where r_i represents the position at time i, and r_0 represents the reference value, r represents the average value of the RMSF, and N represents the number of atoms. The stabilized structure (10–20 ns) was taken from the trajectory of the system to determine the movements of protein backbone and individual residue atoms. The averaged equilibrium rmsd of backbone atom positions and averaged equilibrium RMSF for individual residues were calculated and compared. The differences between the values obtained at 15 and 42 °C for rmsd (ΔRMSD) and RMSF (ΔRMSF) were calculated to provide an estimate of protein flexibility. They are defined as: $\Delta\mathrm{RMSD} = RMSD_{42°C} - RMSD_{15°C}$ and $\Delta\mathrm{RMSF} = RMSF_{42°C} - RMSF_{15°C}$. Differences between species were analyzed by using one-way analysis of variance followed by the Tukey's multiple comparisons test ($P = 0.05$) with GraphPad Prism software (Version 6.0).

1. Dong Y, Somero GN (2009) Temperature adaptation of cytosolic malate dehydrogenases of limpets (genus *Lottia*): Differences in stability and function due to minor changes in sequence correlate with biogeographic and vertical distributions. *J Exp Biol* 212:169–177.
2. Holland LZ, McFall-Ngai M, Somero GN (1997) Evolution of lactate dehydrogenase-A homologs of barracuda fishes (genus *Sphyraena*) from different thermal environments: Differences in kinetic properties and thermal stability are due to amino acid substitutions outside the active site. *Biochemistry* 36:3207–3215.
3. Fields PA, Rudomin EL, Somero GN (2006) Temperature sensitivities of cytosolic malate dehydrogenases from native and invasive species of marine mussels (genus *Mytilus*): Sequence-function linkages and correlations with biogeographic distribution. *J Exp Biol* 209:656–667.
4. Liao ML, et al. (2017) Heat-resistant cytosolic malate dehydrogenases (cMDHs) of thermophilic intertidal snails (genus *Echinolittorina*): Protein underpinnings of tolerance to body temperatures reaching 55°C. *J Exp Biol* 220:2066–2075.
5. Larkin MA, et al. (2007) Clustal W and Clustal X version 2.0. *Bioinformatics* 23:2947–2948.
6. Zhang Y (2008) I-TASSER server for protein 3D structure prediction. *BMC Bioinformatics* 9:40.
7. Phillips JC, et al. (2005) Scalable molecular dynamics with NAMD. *J Comput Chem* 26: 1781–1802.

8. Best RB, et al. (2012) Optimization of the additive CHARMM all-atom protein force field targeting improved sampling of the backbone φ, ψ and side-chain χ(1) and χ(2) dihedral angles. *J Chem Theory Comput* 8:3257–3273.
9. MacKerell AD, Jr, Feig M, Brooks CL, 3rd (2004) Improved treatment of the protein backbone in empirical force fields. *J Am Chem Soc* 126:698–699.
10. MacKerell AD, Jr, et al. (1998) All-atom empirical potential for molecular modeling and dynamics studies of proteins. *J Phys Chem B* 102:3586–3616.
11. Jorgensen WL, Chandrasekhar J, Madura JD, Impey RW, Klein ML (1983) Comparison of simple potential functions for simulating liquid water. *J Chem Phys* 79:926–935.
12. Ryckaert J-P, Ciccotti G, Berendsen HJC (1977) Numerical integration of the cartesian equations of motion of a system with constraints: Molecular dynamics of *n*-alkanes. *J Comput Phys* 23:327–341.
13. Darden T, York D, Pedersen L (1993) Particle mesh Ewald: An N·log(*N*) method for Ewald sums in large systems. *J Chem Phys* 98:10089–10092.
14. Humphrey W, Dalke A, Schulten K (1996) VMD: Visual molecular dynamics. *J Mol Graph* 14:33–38, 27–28.

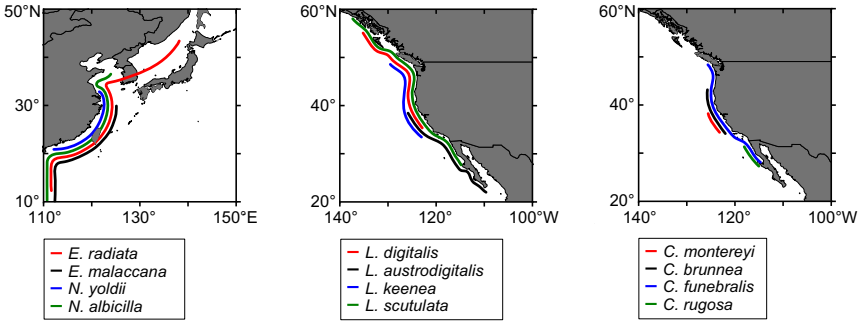

Fig. S1. Map of the biogeographical ranges of the species examined in this study: the snail genus *Echinolittorina* (1–3), snail genus *Nerita* (4–7), snail genus *Littorina* (8, 9), snail genus *Chlorostoma* (10–15), and limpet genus *Lottia* (16–18).

1. Reid DG (2007) The genus *Echinolittorina* Habe, 1956 (Gastropoda: Littorinidae) in the Indo-West Pacific Ocean. *Zootaxa* 1420:1–161.
2. Ma X (2004) Order Mesogastropoda. *Seashells of China*, ed Qi ZY (China Ocean Press, Beijing), pp 31–81.
3. Ohgaki S (1983) Distribution of the family *Littorinidae* (Gastropoda) in Hokkaido, with special emphasis on the distribution in Akkeshi Bay. *Nankiseibutu* 25:173–180.
4. Frey MA (2010) The relative importance of geography and ecology in species diversification: Evidence from a tropical marine intertidal snail (*Nerita*). *J Biogeogr* 37:1515–1528.
5. Frey MA, Vermeij GJ (2008) Molecular phylogenies and historical biogeography of a circumtropical group of gastropods (Genus: *Nerita*): Implications for regional diversity patterns in the marine tropics. *Mol Phylogenet Evol* 48:1067–1086.
6. Crandall ED, Frey MA, Grosberg RK, Barber PH (2008) Contrasting demographic history and phylogeographical patterns in two Indo-Pacific gastropods. *Mol Ecol* 17:611–626.
7. Lin W, Tang YJ, Xiao DP, Cai WQ (2002) The study of fauna and distribution of mollusc in the intertidal zone of Nao Zhou island. *J South China Normal Univ Nat Sci* 3:68–73.
8. Schmitt RJ (1979) Mechanics and timing of egg capsule release by the littoral fringe periwinkle *Littorina planaxis* (Gastropoda: Prosobranchia). *Mar Biol* 50:359–366.
9. Yamada BS (1977) Geographic range limitation of the intertidal gastropods *Littorina sitkana* and *L. planaxis*. *Mar Biol* 39:61–65.
10. Tomanek L, Somero GN (1999) Evolutionary and acclimation-induced variation in the heat-shock responses of congeneric marine snails (genus *Tegula*) from different thermal habitats: Implications for limits of thermotolerance and biogeography. *J Exp Biol* 202:2925–2936.
11. Hellberg ME, Dennis AB, Arbour-Reily P, Aagaard JE, Swanson WJ (2012) The *Tegula* tango: A coevolutionary dance of interacting, positively selected sperm and egg proteins. *Evolution* 66:1681–1694.
12. Hellberg ME (1998) Sympatric sea shells along the sea's shore: The geography of speciation in the marine gastropod *Tegula*. *Evolution* 52:1311–1324.
13. Watanabe JM (1984) The influence of recruitment, competition, and benthic predation on spatial distributions of three species of kelp forest Gastropods (Trochidae: *Tegula*). *Ecology* 65:920–936.
14. Riedman ML, Hines AH, Pearse JS (1981) Spatial segregation of 4 species of turban snails (Gastropoda, *Tegula*) in central California. *Veliger* 24:97–102.
15. Abbott DP, Haderlie EC (1980) Prosobranchia: Marine snails. *Intertidal Invertebrates of California*, eds Morris RH, Abbott DP, Haderlie EC (Stanford Univ Press, Stanford, CA), pp 230–307.
16. Fenberg PB, Rivadeneira MM (2011) Range limits and geographic patterns of abundance of the rocky intertidal owl limpet, *Lottia gigantea*. *J Biogeogr* 38:2286–2298.
17. Lehman JM (2010) Population genetic analysis of the intertidal limpet *Lottia scabra* and inference of the causes and mechanisms of range limits. M.S. dissertation (Univ of California, Merced, CA).
18. Crummett LT, Eernisse DJ (2007) Genetic evidence for the cryptic species pair, *Lottia digitalis* and *Lottia austrodigitalis* and microhabitat partitioning in sympatry. *Mar Biol* 152:1–13.

Other Supporting Information Files

Table S1 (DOCX)
Table S2 (DOCX)
Table S3 (DOCX)
Table S4 (DOCX)
Table S5 (DOCX)